PHYSICAL REVIEW B **90**, 115206 (2014)

Manifestation of two-channel nonlocal spin transport in the shapes of Hanle curves

R. C. Roundy,[1] M. C. Prestgard,[2] A. Tiwari,[2] E. G. Mishchenko,[1] and M. E. Raikh[1]
[1]*Department of Physics and Astronomy, University of Utah, Salt Lake City, Utah 84112, USA*
[2]*Department of Materials Science and Engineering, University of Utah, Salt Lake City, Utah 84112, USA*
(Received 13 August 2014; published 19 September 2014)

The dynamics of charge-density fluctuations in a system of two tunnel-coupled wires contains two diffusion modes with dispersion $i\omega = Dq^2$ and $i\omega = Dq^2 + \frac{2}{\tau_t}$, where D is the diffusion coefficient and τ_t is the tunneling time between the wires. The dispersion of corresponding spin-density modes depends on magnetic field as a result of the spin precession with Larmour frequency ω_L. The presence of two modes affects the shape of the Hanle curve describing the spin-dependent resistance R between the ferromagnetic strips covering the nonmagnetic wires. We demonstrate that the relative shapes of the $R(\omega_L)$ curves, one measured within the same wire and the other measured between the wires, depends on the ratio τ_t/τ_s, where τ_s is the spin-diffusion time. If the coupling between the wires is local, i.e., only at the point $x = 0$, then the difference of the shapes of intrawire and interwire Hanle curves reflects the difference in statistics of diffusive trajectories, which "switch" or do not switch near $x = 0$. When one of the coupled wires is bent into a loop with a radius a, the shape of the Hanle curve reflects the statistics of random walks on the loop. This statistics is governed by the dimensionless parameter $a/\sqrt{D\tau_s}$.

DOI: 10.1103/PhysRevB.90.115206 PACS number(s): 72.25.Dc, 75.40.Gb, 73.50.−h, 85.75.−d

I. INTRODUCTION

Spin-orbit interaction is the origin of spin dephasing in semiconductors and metals. On a microscopic level, a finite spin-relaxation time τ_s results from the momentum-dependent spin-orbit term in the Hamiltonian of a free electron in combination with scattering-induced momentum relaxation [1]. In metals, the origin of spin dephasing is spin-dependent impurity scattering.

The first experimental studies [2–4] of spin relaxation in semiconductors were carried out more than four decades ago. They were based on the notion that if the photoexcited electron has its spin pointing along the x axis, then in a magnetic field ω_L, directed along the z axis, the projection $S_x(t)$ evolves as $S_x(t) = \cos\omega_L t \exp(-t/\tau_s)$, which is the result of the Larmour precession. Since the time between generation and recombination is much longer than τ_s, so that the spin evolution is completed by the moment of recombination, then the polarization of the luminescence is proportional to $\int_0^\infty dt\, S_x(t)$, i.e.,

$$\mathcal{P}(\omega_L) = \frac{\mathcal{P}(0)}{1+\omega_L^2\tau_s^2}. \tag{1}$$

Numerous experimental measurements reported to date can be fit very accurately with a Lorentzian Hanle profile, Eq. (1), and when they do not, see, e.g., Ref. [5], the deviations reflect the peculiarity of the recombination process.

In the pioneering work of Refs. [6,7], it was demonstrated that, aside from optics, the underlying physics of spin relaxation manifests itself in transport experiments. The structure fabricated and measured in Ref. [6] represented an aluminum wire with two cobalt ferromagnetic strips on the top. The first strip, injector, played the role of circular-polarized excitation light in optics, in the sense, that it supplied spin-polarized electrons into the wire. Correspondingly, the second strip, the detector, imitated the analyzer of the emitted light. The characteristic measured in Ref. [6] was the nonlocal resistance R, which is the ratio of the voltage, generated between the channel and detector, to the current passed through the injector into the channel.

Similar to the polarization of luminescence $\mathcal{P}(\omega_L)$, the nonlocal resistance is suppressed with an external field ω_L. There is, however, a fundamental difference between the dependencies $\mathcal{P}(\omega_L)$ and $R(\omega_L)$. This difference stems from the fact that, in addition to the Larmour precession, the formation of nonlocal resistance involves diffusion of carriers over a distance L between the injector and the detector. This diffusion is routinely incorporated into the theory by multiplying $\cos\omega_L t \exp(-t/\tau_s)$ by a diffusion propagator $P_L(t)$ and only, subsequently, integrating over time. In one dimension, $P_L(t)$ has the form

$$P_L(t) = \frac{1}{(4\pi Dt)^{1/2}} \exp\left(-\frac{L^2}{4Dt}\right), \tag{2}$$

where D is the diffusion coefficient.

The nonlocal resistance $R(\omega_L)$, calculated with the help of propagator (2), is also called the Hanle curve in the literature. The expression for $R(\omega_L)$ contains two unknown parameters, τ_s and D. Still it appears that the scores of experimental data accumulated to date can be fitted very accurately with this expression. It is apparent that the shapes of $R(\omega_L)$ is different for "short" $L \ll (D\tau_s)^{1/2}$ and long $L \gg (D\tau_s)^{1/2}$ samples. This difference in shapes was pointed out already in the seminal paper of Ref. [6], where the two samples measured had the lengths $L = 50$ and 300 μm.

Experimental studies of nonlocal spin transport became a hot topic in 2001 when the measurements of $R(\omega_L)$ were reported [8] for small samples with $L \sim 0.5$ μm. Small structures are appealing for information-storage applications. Indeed, the effect of sign reversal of nonlocal resistance upon reversal of the magnetization of the detector allows one to view the detector as an element of information storage. For this reason, the $R(\omega_L)$ measurements in spin transport were carried out since 2001 on various structures with L in the micrometer range and with materials of nonmagnetic channels ranging from Si and GaAs, see, e.g., Refs. [9,10], to graphene [11], and organic materials [12].

It turns out that the scope of the experimental results on nonlocal resistance is described by the drift-diffusion theory with remarkable precision and including finest details, see, e.g., Refs. [9,13–16]. For example, in long samples $L \gg (D\tau_s)^{1/2}$, the theory predicts several zeros in $R(\omega_L)$ dependence. The origin of these zeros is that during the time L^2/D of travel between the injector and detector the spin can precess by 2π, 4π, and so on. Clearly, the values of $R(\omega_L)$ between these zeros fall off dramatically. Then the number of the zeros observed in the experimental $R(\omega_L)$ attests to the accuracy with which the theory captures the process of spin transport. Usually, only the first zero is resolved in experiment. However, the very recent data in Ref. [16] exhibit the second zero as well.

To illustrate the accuracy with which the drift-diffusion theory works for spin-transport devices with variable channel length, in Figs. 1(b) and 1(c), we plot the Hanle shapes measured for two devices fabricated from epitaxial ZnO films. Both devices were fabricated under the same conditions [17], which included pulsed-laser deposition of ZnO onto a sapphire substrate, deposition of a thin barrier layer of MgO on top, and, finally, the deposition of NiFe electrodes using photolithography and e-beam evaporation. The only difference between the two devices was the distance between the contacts ($L = 90$ and 650 nm) in the four-probe structure, see Fig. 1(a). We see that the seven-fold increase in L changes the shape dramatically, in *quantitative* agreement with predictions of the drift-diffusion theory.

The fact that the measured $R(\omega_L)$ is so accurately described by the drift-diffusion theory suggests that the shape of the Hanle curve is the characteristics of the spin transport in nonmagnetic channel only, and is not affected by the details of injection and detection. It also suggests that the description of electron diffusion paths as purely one-dimensional is surprisingly adequate. In fact, in experimental geometries, the length L of the channel does not exceed significantly the channel width.

This motivated us to study theoretically the shapes of the Hanle curves in geometries when the transport between the injector and detector does not reduce to a 1D random walk. The results of this study are reported in Secs. II and III, where we consider the spin transport along two parallel tunnel-coupled wires. In Sec. IV, we analyze the shapes of the Hanle curves for the geometry of two wires coupled locally. In Sec. V, we consider the special case when one of the wires is bent into a loop. Concluding remarks are presented in Sec. VI.

Our objective was to find out whether the statistics of diffusion paths, specific for quasi-1D geometries, can be distinguished in nonlocal spin-transport measurements. Our main message is that the difference of the Hanle curves measured with two detectors, one located in the same wire as injector and the other located in the neighboring wire, reflects the peculiar statistics of the diffusion paths in a coupled system.

II. SPIN-DENSITY FLUCTUATIONS IN TUNNEL-COUPLED WIRES

Fluctuations of electron densities, $n_1(x,t)$ and $n_2(x,t)$, in a system of two coupled wires satisfy the system of equations

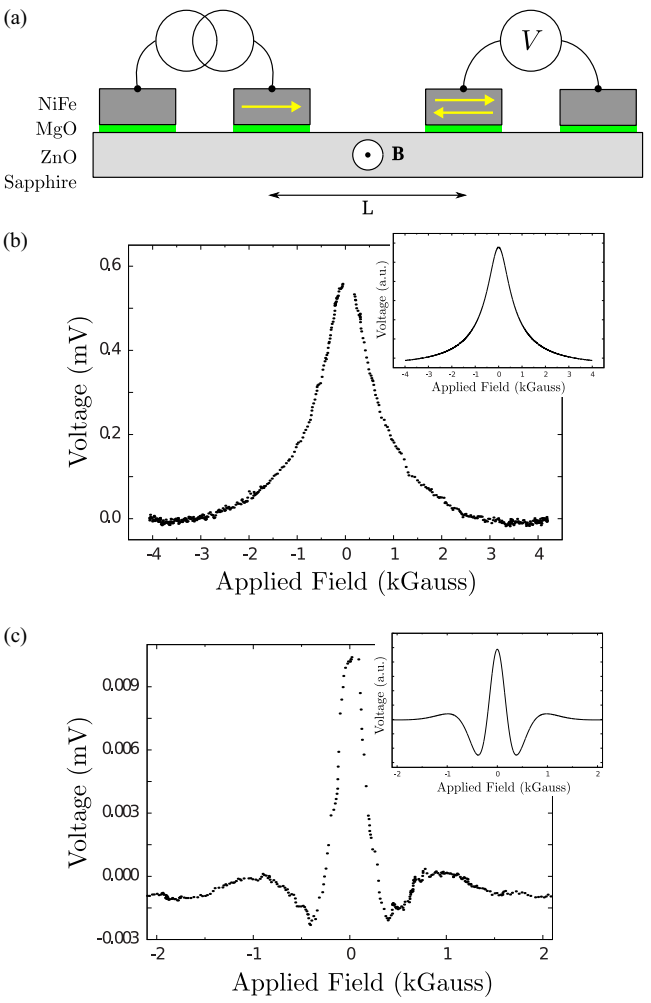

FIG. 1. (Color online) (a) Schematic view of a four-terminal device used for nonlocal spin-transport measurements [17]. Epitaxial ZnO film of thickness 200 nm, deposited on a sapphire substrate, is spaced from a NiFe layer by a thin MgO barrier; (b) and (c) Hanle curves measured for the channel length $L = 90$ and 650 nm, respectively. The insets show the theoretical fits plotted from Eqs. (17), (18), (24), and (26). The values τ_s used for both fits are the same, so that the dimensionless lengths $\mathcal{L} = L/\sqrt{4D\tau_s}$ differ seven times.

[18]

$$\frac{\partial n_1}{\partial t} = D\frac{\partial^2 n_1}{\partial x^2} - \frac{1}{\tau_t}(n_1 - n_2),$$
$$\frac{\partial n_2}{\partial t} = D\frac{\partial^2 n_2}{\partial x^2} - \frac{1}{\tau_t}(n_2 - n_1), \tag{3}$$

where τ_t is the interwire tunneling time. We assume that the wires are disordered so that $\tau_t \gg \tau$, where τ is the disorder-scattering time. The latter condition implies that the tunnel splitting Δ_t of the spectra of the wires in the absence of disorder is much smaller than τ_t^{-1}. In this limit, the expression for τ_t reads [19,20]

$$\tau_t = \frac{1}{\Delta_t^2 \tau}. \tag{4}$$

Upon introducing the variables

$$n_{\pm}(x) = n_1(x) \pm n_2(x), \tag{5}$$

we find that Eq. (3) gives rise to two modes with dispersions

$$i\omega = Dq^2, \quad i\omega = Dq^2 + \frac{2}{\tau_t} \tag{6}$$

corresponding to symmetric and antisymmetric distributions of densities, respectively. The fact that the antisymmetric mode is gapped indicates that the contribution to transport from this mode cannot be described by a simple diffusion used in the theory of the Hanle effect. This is because the propagator (2), describing the statistics of the location of a carrier in time and in space, no longer applies.

The actual distributions $n_1(x,t)$ and $n_2(x,t)$ are linear combinations of symmetric and antisymmetric modes with weights determined by the initial conditions. If electrons are injected into the first wire at $x = 0$, the combinations satisfying the initial conditions

$$n_1(x,0) = \delta(x), \quad n_2(x,0) = 0 \tag{7}$$

are the sum and the difference of two diffusion modes:

$$\begin{aligned} n_1(x,t) &= \tfrac{1}{2} P_x(t)(1 + e^{-2t/\tau_t}), \\ n_2(x,t) &= \tfrac{1}{2} P_x(t)(1 - e^{-2t/\tau_t}), \end{aligned} \tag{8}$$

where the diffusion propagator $P_x(t)$ is defined by Eq. (2).

To describe the nonlocal resistance we need the expressions for the spin densities, $\boldsymbol{S}_1(x,t)$ and $\boldsymbol{S}_2(x,t)$, similar to Eq. (8). The system of coupled equations for $\boldsymbol{S}_1(x,t)$, $\boldsymbol{S}_2(x,t)$ has the form

$$\begin{aligned} \frac{\partial \boldsymbol{S}_1}{\partial t} &= \boldsymbol{\omega}_L \times \boldsymbol{S}_1 - \frac{\boldsymbol{S}_1}{\tau_s} + D\frac{\partial^2 \boldsymbol{S}_1}{\partial x^2} - \frac{1}{\tau_t}(\boldsymbol{S}_1 - \boldsymbol{S}_2), \\ \frac{\partial \boldsymbol{S}_2}{\partial t} &= \boldsymbol{\omega}_L \times \boldsymbol{S}_2 - \frac{\boldsymbol{S}_2}{\tau_s} + D\frac{\partial^2 \boldsymbol{S}_2}{\partial x^2} - \frac{1}{\tau_t}(\boldsymbol{S}_2 - \boldsymbol{S}_1), \end{aligned} \tag{9}$$

and differs from the corresponding equations Eq. (3) describing the charge-density fluctuations in two aspects: both $\boldsymbol{S}_1$ and $\boldsymbol{S}_2$, precess in magnetic field, $\boldsymbol{\omega}_L$, and both decay during the spin relaxation time τ_s,

$$\tau_s = \frac{1}{\Delta_s^2 \tau}, \tag{10}$$

where Δ_s is the spin-orbit splitting of the spectrum in each wire in the absence of disorder. Note that, while both τ_t and τ_s contain scattering time, the ratio τ_s/τ_t does not contain disorder, i.e., it is a characteristics of clean wires. The term coupling the wires in the system, Eq. (9), has the same form as in the system (3) since tunneling conserves the spin.

By choosing for τ_s the form (10) we specified the dominant spin relaxation mechanism as Dyakonov-Perel [1]. The fact that the expression for Eq. (4) for τ_t has a similar form is not a coincidence. Indeed, the degenerate states in the wires can be viewed as a pseudospin. Due to finite Δ_t, the electron density exercises the "beatings," $\cos \Delta_t t$, between the wires, in the same way as real spin precesses in a spin-orbit field. Finally, both processes are terminated after the scattering time, τ.

Without boundary conditions, the system (9) defines four modes:

$$i\omega = -Dq^2 - \frac{1}{\tau_s} \pm i\omega_L, \quad i\omega = -Dq^2 - \frac{1}{\tau_s} - \frac{2}{\tau_t} \pm i\omega_L, \tag{11}$$

of which the first two correspond to symmetric and the second two to the antisymmetric spin-density fluctuations. With boundary conditions, the solution of the system (9) can be expressed in terms of the solution (8) of Eq. (3) as follows:

$$\boldsymbol{S}_1(x,t) = \boldsymbol{s}(t) n_1(x,t), \quad \boldsymbol{S}_2(x,t) = \boldsymbol{s}(t) n_2(x,t), \tag{12}$$

where the function $\boldsymbol{s}(t)$ satisfies the conventional equation of spin dynamics,

$$\frac{d\boldsymbol{s}}{dt} = \boldsymbol{\omega}_L \times \boldsymbol{s} - \frac{\boldsymbol{s}}{\tau_s}. \tag{13}$$

III. NONLOCAL RESISTANCES

The initial condition to Eq. (13) is set by the direction of the polarization of the injector. We assume that $\boldsymbol{s}(0)$ is directed along the x axis.

As it is illustrated in Fig. 2, there are two nonlocal resistances: $R_{11}(\omega_L)$ is the resistance measured by the detector within the same wire, 1, where polarized electrons are injected, and R_{12} is the resistance measured by the detector that covers

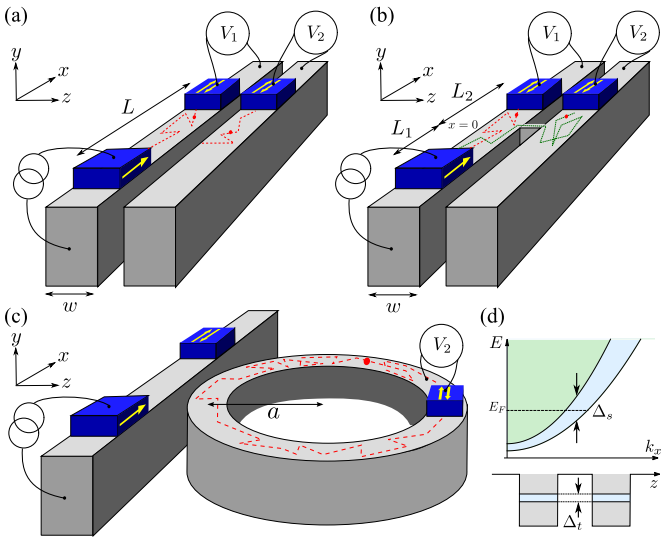

FIG. 2. (Color online) (a) Two-channel spin-transport device. The injector is located in the left channel. Two detectors in the left and right channels are located at the same distance L from the injector. An electron reaches the first detector by diffusion and the second detector by a combined diffusion-tunneling process. (b) In contrast to (a), two channels are coupled *locally* at the point $x = 0$; (c) the second wire is bent into a loop. Electron diffusion trajectories encircle the loop several times before the spin polarization is "forgotten"; (d) two branches, $E(k_x)$, of the energy spectrum of the tunnel-coupled wires. At small momenta, the splitting Δ_t is determined by tunneling, while at large k_x the splitting Δ_s is dominated by the spin-orbit coupling in the wires.

the wire 2. Within a prefactor they are given by

$$\mathcal{R}_{11} = R_0 L \int_0^\infty \frac{dt}{\tau_s} S_{1x}(L,t),\ \mathcal{R}_{12} = R_0 L \int_0^\infty \frac{dt}{\tau_s} S_{2x}(L,t). \tag{14}$$

In Eq. (14), it is implicit that the magnetization of the detector is also along the x axis. In some experiments, say Ref. [21], the spin transport was studied for the polarization of the detector along the y axis. The corresponding expression for nonlocal resistance reads

$$\widetilde{\mathcal{R}}_{11} = R_0 L \int_0^\infty \frac{dt}{\tau_s} S_{1y}(L,t),\ \widetilde{\mathcal{R}}_{12} = R_0 L \int_0^\infty \frac{dt}{\tau_s} S_{2y}(L,t). \tag{15}$$

Our goal is to find the expressions for $\mathcal{R}_{11}(\omega_L)$ and $\mathcal{R}_{12}(\omega_L)$ for two tunnel-coupled wires. One can see that the coupling strength τ_t^{-1} enters into the formulas for $\mathcal{R}_{11}(\omega_L)$, $\mathcal{R}_{12}(\omega_L)$ through the last terms in Eq. (3). These terms decay exponentially with time. We also notice that $\boldsymbol{s}(t)$, which satisfies Eq. (13) is also an exponential function of time. This observation allows one to express $\mathcal{R}_{11}(\omega_L)$, $\mathcal{R}_{12}(\omega_L)$ with tunneling through nonlocal resistance, $R(\omega_L)$, *in the absence of tunneling*.

Setting $\tau_t = \infty$ and substituting

$$\boldsymbol{s}(t) = e^{-t/\tau_s}(\boldsymbol{i}\ \cos\omega_L t + \boldsymbol{j}\sin\omega_L t) \tag{16}$$

into Eq. (12) and, subsequently, into Eq. (14), we restore a standard expression for the Hanle profile of a single channel:

$$R(\omega_L,\tau_s) = R_0 F(\omega_L,\tau_s), \tag{17}$$

where the dimensionless function $F(\omega_L,\tau_s)$ is defined as

$$F(\omega_L,\tau_s) = \frac{L}{\tau_s}\int_0^\infty dt \cos\omega_L t e^{-t/\tau_s} P_L(t), \tag{18}$$

so that R_0 has the dimensionality of the resistance.

Then, in terms of the function $R(\omega_L,\tau_s)$, the final result for nonlocal resistances can be presented as

$$\mathcal{R}_{11} = \frac{1}{2}\left[R(\omega_L,\tau_s) + \frac{\tilde{\tau}_s}{\tau_s}R(\omega_L,\tilde{\tau}_s)\right],$$
$$\mathcal{R}_{12} = \frac{1}{2}\left[R(\omega_L,\tau_s) - \frac{\tilde{\tau}_s}{\tau_s}R(\omega_L,\tilde{\tau}_s)\right], \tag{19}$$

where $\tilde{\tau}_s$ is an effective spin relaxation time

$$\tilde{\tau}_s = \frac{\tau_s\tau_t}{2\tau_s+\tau_t}, \tag{20}$$

which includes tunneling and is shorter than τ_s. Modifications of the Hanle curves due to tunneling are analyzed below.

A. Limiting cases

As it was mentioned in Introduction, the shape of the Hanle curve for a single wire is governed by the dimensionless length

$$\mathcal{L} = \frac{L}{\sqrt{4D\tau_s}}. \tag{21}$$

(i) It is apparent that when both wires are long, $\mathcal{L} \gg 1$, the shapes of the curves $\mathcal{R}_{11}$ and $\mathcal{R}_{12}$ do not differ significantly, since a typical electron will have enough time to tunnel before it reaches one of two detectors.

(ii) It is also obvious on general grounds that when the tunneling time is much shorter than the spin-relaxation time, $\tau_t \ll \tau_s$, the nonlocal resistance $\mathcal{R}_{11}$ exceeds $\mathcal{R}_{12}$ only slightly. This is because the electron gets equally distributed between the wires before the spin precession takes place. Formally, this follows from Eqs. (19) and (20). In the limit $\tau_t \ll \tau_s$, one has $\tilde{\tau}_s \approx \tau_t/2$. The relative difference, $(\mathcal{R}_{11}-\mathcal{R}_{12})/\mathcal{R}_{11}$, is of the order of $(\tau_t/\tau_s)^{1/2}$.

(iii) The opposite limit of weak tunneling between the wires is most insightful. In this limit, we have $\tau_t \gg \tau_s$, so that only a small portion of electrons injected in the first wire reach the detector in the second wire. This means that $\mathcal{R}_{12}$, is much smaller than $\mathcal{R}_{11}$. Formally, two terms in Eq. (19) for $\mathcal{R}_{12}$ nearly cancel each other. However, $\mathcal{R}_{12}(\omega_L)$ possesses a distinctive shape. To find this shape, we expand Eq. (19) with respect to τ_s/τ_t and get

$$\mathcal{R}_{12} \approx R_0\frac{\tau_s}{\tau_t}G(\omega_L,\tau_s), \tag{22}$$

where the function $G(\omega_L,\tau_s)$ is defined as

$$G(\omega_L,\tau_s) = \frac{L}{\tau_s^2}\int_0^\infty dt\ t\cos\omega_L t e^{-t/\tau_s} P_L(t). \tag{23}$$

Analytical expressions for $F(\omega_L,\tau_s)$ and $G(\omega_L,\tau_s)$ for arbitrary length can be found using the identities

$$\int_0^\infty \frac{ds}{s^{1/2}}\exp\left(-\frac{1}{s}-ys\right) = \left(\frac{\pi}{y}\right)^{1/2}\exp\left(-2y^{1/2}\right), \tag{24}$$

$$\int_0^\infty ds s^{1/2}\exp\left(-\frac{1}{s}-ys\right) = \frac{\pi^{1/2}}{2y^{3/2}}(1+2y^{1/2})\exp(-2y^{1/2}), \tag{25}$$

and taking the absolute value and the phase of the complex argument y to be

$$|y| = \mathcal{L}^2\left(1+\omega_L^2\tau_s^2\right)^{1/2},\quad \phi = \arctan(\omega_L\tau_s). \tag{26}$$

In Fig. 3, we plot these functions that represent the Hanle curves for diagonal and nondiagonal resistances for three domains of $\mathcal{L}$. It is seen, Fig. 3(a), that for large length the shapes of both curves are identical. The smaller is the length the more pronounced is the difference between $\mathcal{R}_{11}$ and $\mathcal{R}_{12}$ behaviors. The $\mathcal{R}_{12}(\omega_L)$ curve is significantly narrower than $\mathcal{R}_{11}(\omega_L)$ for small length, as it is seen in Fig. 3(c). This narrowing originates from the extra factor t in the integrand of Eq. (23) compared to Eq. (18) and can be qualitatively interpreted as follows. In order to reach the detector in the second wire, injected electron diffuses along the first wire, tunnels into the second wire, and diffuses there. Narrower shape indicates that reaching the detector in the second wire takes more time than reaching the detector in the first wire to which electron simply diffuses.

(iv) Note that the limit of short wires allows a comprehensive analytical study to which we now turn. In the limit of small wire length, $\mathcal{L} \ll 1$, analytical expressions for $\mathcal{R}_{11}$ and $\mathcal{R}_{12}$ can be obtained for an arbitrary relation between τ_t and τ_s. In this limit, corresponding to $|y| \ll 1$ in Eq. (24), the expression for nonlocal resistances, $R(\omega_L,\tau_s)$ and $\tilde{R}(\omega_L,\tau_s)$ of an isolated

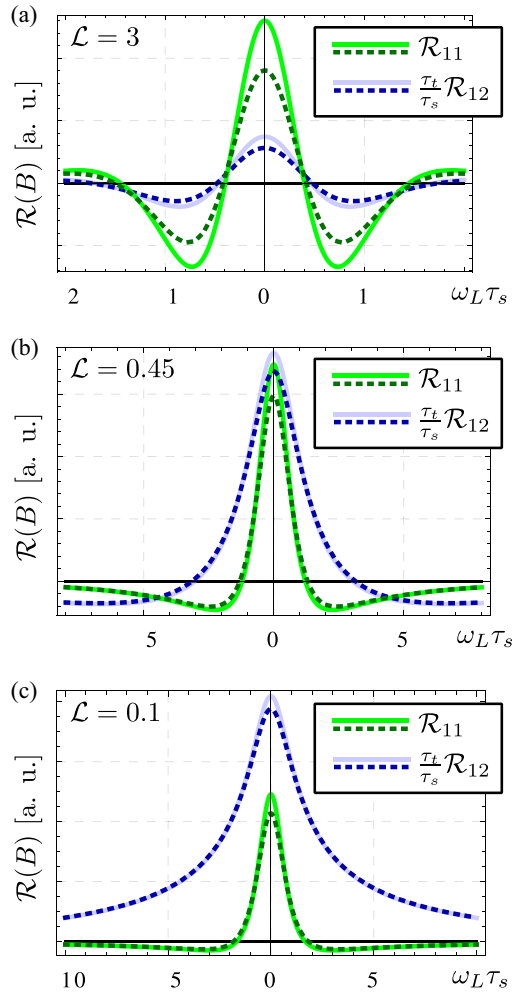

FIG. 3. (Color online) Hanle curves $\mathcal{R}_{11}(\omega_L)$ (blue) and $\mathcal{R}_{12}(\omega_L)$ (green) measured by two detectors, one located in the same wire as the injector and the other located in the neighboring wire. Dashed curves are plotted directly from Eq. (19) using the definition (17); the solid curves are plotted from the asymptotic expansions, $\mathcal{R}_{11}$ is given by Eq. (18) and $\mathcal{R}_{12}$ is given by Eq. (22). In all graphs, the tunneling time τ_t is $10\tau_s$. The three panels correspond to different dimensionless lengths, $\mathcal{L} = L/\sqrt{4D\tau_s}$: $\mathcal{L} = 3$ (a), $\mathcal{L} = 0.45$ (b), and $\mathcal{L} = 0.1$ (c). All curves for $\mathcal{R}_{12}$ are multiplied by $\tau_t/\tau_s = 10$.

wire simplify to

$$R(\omega_L,\tau_s) = \frac{R_0\mathcal{L}}{\sqrt{2}}\frac{\sqrt{\sqrt{1+\omega_L^2\tau_s^2}+1}}{\sqrt{1+\omega_L^2\tau_s^2}}, \tag{27}$$

$$\tilde{R}(\omega_L,\tau_s) = \frac{R_0\mathcal{L}}{\sqrt{2}}\frac{\sqrt{\sqrt{1+\omega_L^2\tau_s^2}-1}}{\sqrt{1+\omega_L^2\tau_s^2}}. \tag{28}$$

Here, $\tilde{R}(\omega_L,\tau_s)$ is naturally defined by Eqs. (17) and (18), namely, upon replacing $\cos\omega_L t$ by $\sin\omega_L t$ in the integrand. Substituting Eq. (27) into Eq. (19), we get

$$\begin{pmatrix}\mathcal{R}_{11}(\omega_L)\\ \mathcal{R}_{12}(\omega_L)\end{pmatrix} = \frac{R_0\mathcal{L}}{2\sqrt{2}}\left[\frac{\sqrt{\sqrt{1+\omega_L^2\tau_s^2}+1}}{\sqrt{1+\omega_L^2\tau_s^2}} \pm\sqrt{\frac{\tilde{\tau}_s}{\tau_s}}\frac{\sqrt{\sqrt{1+\omega_L^2\tilde{\tau}_s^2}+1}}{\sqrt{1+\omega_L^2\tilde{\tau}_s^2}}\right]. \tag{29}$$

The second term in Eq. (29) is responsible for the difference between $\mathcal{R}_{11}$ and $\mathcal{R}_{12}$. It is apparent that this difference is maximal when $\tilde{\tau}_s \approx \tau_s$, i.e., when the tunneling time is long. In the latter case, we can simplify Eq. (29) further by expanding with respect to τ_s/τ_t:

$$\mathcal{R}_{12} = \frac{R_0\mathcal{L}}{2\sqrt{2}}\frac{\tau_s}{\tau_t}\frac{1}{\left(1+\omega_L^2\tau_s^2\right)^{3/2}}\frac{\sqrt{1+\omega_L^2\tau_s^2}+1-\omega_L^2\tau^2}{\sqrt{\sqrt{1+\omega_L^2\tau_s^2}+1}}. \tag{30}$$

Now $\mathcal{R}_{12}$ is a function of a single argument, $\omega_L\tau_s$. We see that, while $\mathcal{R}_{11}$ falls off at large $\omega_L\tau_s$ as $(\omega_L\tau_s)^{-1/2}$, the decay of $\mathcal{R}_{12}$ is much faster, as $(\omega_L\tau_s)^{-3/2}$. Besides, the distinctive feature of $\mathcal{R}_{12}$ is that it passes through zero at $\omega_L\tau_s = \sqrt{3}$. Overall, see Fig. 3, despite that the length is small, the behavior of nondiagonal resistance $\mathcal{R}_{12}$ resembles the shape of the Hanle curve for a long wire, $\mathcal{L} \gg 1$.

IV. LOCAL COUPLING

A different arrangement of two coupled wires is shown in Fig. 2(b). Electron injected into the first wire can cross into the second wire only through a narrow bridge at $x = 0$. This means that, while $\mathcal{R}_{11}$ is constituted by all diffusive trajectories in the first wire, the contribution to $\mathcal{R}_{12}$ comes from a subset of diffusive trajectories, which visit the point of contact. More precisely, the bridge serves as "weak" boundary condition for the diffusion equation. We are going to study how this modification of the diffusion due to crossing into neighboring wire affects the shape of the Hanle curve, $\mathcal{R}_{12}$, and compare the result with $\mathcal{R}_{12}(\omega_L)$ calculated for homogeneous tunneling in the previous section.

We assume that the coupling via the bridge is weak, so that the concentration $n_1(x,t)$ is given by $P_{x+L_1}(t)$. The presence of the bridge in the diffusion equation (3) for $n_2(x,t)$ is reflected as a source,

$$\frac{\partial n_2}{\partial t} - D\frac{\partial^2 n_2}{\partial x^2} = \frac{l}{\tau_t}\delta(x)n_1(0,t), \tag{31}$$

where $l \ll L$ represents the width of the bridge. The solution of Eq. (31) can be obtained in a standard way, e.g., by the Fourier expansion of both sides. The expression for $n_2(x,t)$ reads

$$n_2(x,t) = \frac{l}{\tau_t}\int_0^t dt_1 P_x(t-t_1)n_1(0,t_1). \tag{32}$$

Substituting the expression for $n_1(0,t)$ into the integrand, we cast the final result in the form

$$n_2(x,t) = \frac{l}{\tau_t}\int_0^t dt_1 \int_0^t dt_2 P_x(t_1)P_{L_1}(t_2)\delta(t_1+t_2-t), \quad (33)$$

which is simply the convolution of two diffusion propagators. Physically, the result (33) is transparent. It expresses the fact that, to get to the point x in the second wire, an electron first diffuses from the injector to the bridge and then from the bridge to the point x.

The form (33) is convenient for the calculation of the nonlocal resistance $\mathcal{R}_{12}(\omega_L)$. Indeed, for this calculation one has to multiply $n_2(x,t)$ by $s(t)$, given by Eq. (16), and integrate over t, which leads to the expression

$$\mathcal{R}_{12}(\omega_L) = R_0 L \int_0^\infty dt\ n_2(L_2,t)e^{-t/\tau_s}\cos\omega_L t. \quad (34)$$

Substituting Eq. (33) into Eq. (34) and performing integration over time with the help of the δ function, we get

$$\mathcal{R}_{12}(\omega_L) = \frac{R_0(L_1+L_2)l}{\tau_t\tau_s}\int_0^\infty dt_1\int_0^\infty dt_2\ P_{L_1}(t_1)P_{L_2}(t_2) \times e^{-(t_1+t_2)/\tau_s}(\cos\omega_L t_1\cos\omega_L t_2 - \sin\omega_L t_1\sin\omega_L t_2). \quad (35)$$

We now notice that, for both terms in the brackets, the double integral (35) factorizes into a product of single integrals, which, in turn, can be expressed through the functions $R(\omega_L)$ and $\tilde{R}(\omega_L)$ for a *single* wire. The final expression for $\mathcal{R}_{12}(\omega_L)$ reads

$$\mathcal{R}_{12} = \frac{\tau_s}{\tau_t}\frac{(L_1+L_2)l}{L_1L_2}\frac{1}{R_0} \times (R(\omega_L,L_1)R(\omega_L,L_2) - \tilde{R}(\omega_L,L_1)\tilde{R}(\omega_L,L_2)). \quad (36)$$

Similarly, for orthogonal magnetizations of injector and detector we get

$$\widetilde{\mathcal{R}}_{12} = \frac{\tau_s}{\tau_t}\frac{(L_1+L_2)l}{L_1L_2}\frac{1}{R_0} \times (R(\omega_L,L_1)\tilde{R}(\omega_L,L_2) + \tilde{R}(\omega_L,L_1)R(\omega_L,L_2)). \quad (37)$$

According to Eq. (36), $\mathcal{R}_{12}$ depends on *both* the position of the bridge and the position of the detector. In Appendix, we demonstrate that the dependence of the concentration, $n_2(L_2,t)$, on the position of the bridge drops out, so that $\mathcal{R}_{12}$ only depends only on the distance, $L = L_1 + L_2$ between the injector and the detector. This observation allows L_2 to be set to zero in Eq. (36); correspondingly, L_1 should be set equal to the total length L. Technically, this implies that we can use the short-distance asymptotes, Eq. (27) and Eq. (28), while for $R(\omega_L,L)$ and $\tilde{R}(\omega_L,L)$ the general expressions should be used. These general expressions [8,22] follow from Eq. (24):

$$R(\omega_L,L) = \left(\frac{\pi}{|y|}\right)^{1/2}\exp\left(-2|y|^{1/2}\cos\frac{\phi}{2}\right) \times \cos\left(\frac{\phi}{2}+2|y|^{1/2}\sin\frac{\phi}{2}\right), \quad (38)$$

where the magnitude $|y|$, and phase ϕ, are defined by Eq. (26). The corresponding expression for $\tilde{R}(\omega_L,L)$ differs from Eq. (38) by the replacement of cos with sin in the second factor.

Summarizing, in the geometry of two wires with a bridge, the Hanle curve measured by the first detector is described by $R(\omega_L,L)$, Eq. (38), while the Hanle curve measured by the second detector has the shape given by

$$\mathcal{R}_{12} \propto \frac{\tau_s}{\tau_t}\frac{l}{L}\left(\frac{\sqrt{\sqrt{1+\omega_L^2\tau_s^2}+1}}{\sqrt{1+\omega_L^2\tau_s^2}}R(\omega_L,L) - \frac{\sqrt{\sqrt{1+\omega_L^2\tau_s^2}-1}}{\sqrt{1+\omega_L^2\tau_s^2}}\tilde{R}(\omega_L,L)\right). \quad (39)$$

The most dramatic difference in the shapes of two Hanle curves emerges in the limit of short wires, $\mathcal{L} \ll 1$. Substituting Eqs. (27) and (28) into Eq. (39), we get the amusingly simple expressions for $\mathcal{R}_{12}$, $\tilde{\mathcal{R}}_{12}$

$$\mathcal{R}_{12} = \frac{1}{1+\omega_L^2\tau_s^2}, \quad \tilde{\mathcal{R}}_{12} = \frac{\omega_L\tau_s}{1+\omega_L^2\tau_s^2}. \quad (40)$$

This means that, while the first detector measures the shape, Eq. (27), the second detector measures a simple Lorentzian, Eq. (1), as in optical measurements. In Figs. 4(a) and 4(b), this difference in shapes is illustrated graphically for $\mathcal{R}_{12}$ and $\tilde{\mathcal{R}}_{12}$, respectively. We see that $\mathcal{R}_{12}$ in the second wire is not only narrower, but also possesses a distinctively different shape. Figure 4(c) illustrates that the difference in the shapes of the two Hanle curves gradually vanished as the wires get longer. Qualitatively, this can be understood from Eq. (39). In a long wire, the Hanle curve is narrow. This allows us to set $\omega_L\tau_s \ll 1$ in the prefactors in the brackets. Then the first prefactor is close to 1, while the second prefactor is much smaller. Thus we conclude that the ratio of $\mathcal{R}_{12}$ to $\mathcal{R}_{11}$ is approximately constant.

V. COUPLING OF A WIRE TO THE LOOP

As a last example of the modification of the Hanle profile with restricted geometry consider a loop tunnel-coupled to a wire, see Fig. 2. The injector is located in the wire while the detector is located in the loop. The spin-transport equation has a form

$$\frac{\partial}{\partial t}\boldsymbol{S}(\theta,t) = \boldsymbol{\omega}_L \times \boldsymbol{S}(\theta,t) + \frac{D}{a^2}\frac{\partial^2}{\partial\theta^2}\boldsymbol{S}(\theta,t) - \frac{\boldsymbol{S}(\theta,t)}{\tau_s}, \quad (41)$$

where θ is the azimuthal coordinate and a is the radius of the loop. This equation also allows a factorization: $\boldsymbol{S}(\theta,t) = \boldsymbol{s}(t)n(\theta,t)$, where $\boldsymbol{s}(t)$ satisfies Eq. (13), while the equation for

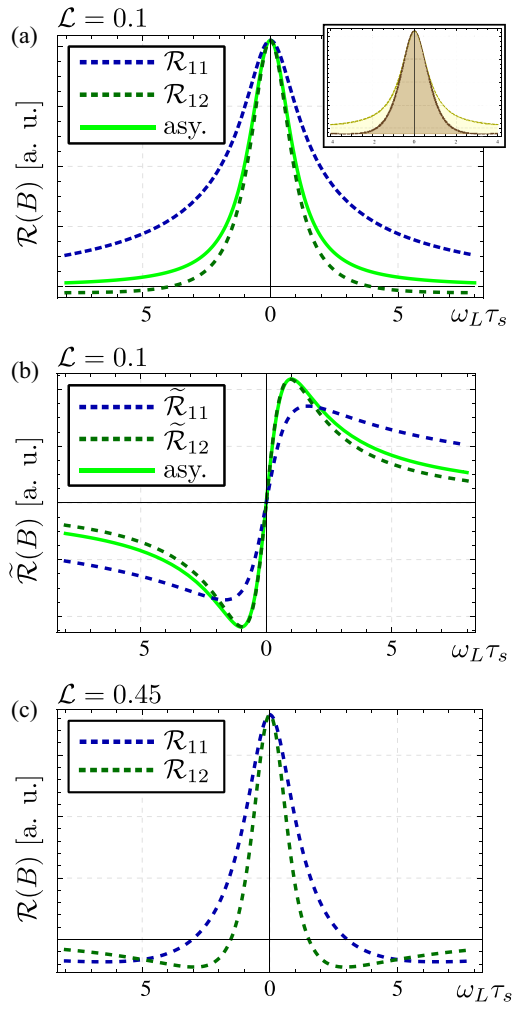

FIG. 4. (Color online) The difference in the diffusion trajectories in a single wire and in two wires coupled via a bridge manifests itself in the shapes of the Hanle curves. (a) The Hanle curves $\mathcal{R}_{11}(\omega_L)$ (blue) and $\mathcal{R}_{12}(\omega_L)$ (green, dashed) are plotted from Eqs. (38) and (39) for a small dimensionless length $\mathcal{L} = L/(4D\tau_s)^{1/2} = 0.1$. The solid green curve is the Lorentzian asymptote, Eq. (40). The inset shows a comparison of $\mathcal{R}_{12}(\omega_L)$ for the case of local tunneling (yellow), Eq. (40), and for the case of homogeneous tunneling (brown), Eq. (30); (b) same geometry as in (a). Nondiagonal components of nonlocal resistance corresponding to the perpendicular magnetizations of injector and detector are plotted; (c) the Hanle curve $\mathcal{R}_{11}(\omega_L)$ (blue) and $\mathcal{R}_{12}(\omega_L)$ (green) are plotted for the dimensionless length $\mathcal{L} = 0.45$. The shapes are much closer than in (a).

$n(\theta,t)$ reads

$$\frac{\partial n}{\partial t} = \frac{D}{a^2}\frac{\partial^2 n}{\partial \theta^2}. \tag{42}$$

The solution of this equation satisfying the initial condition, $n(\theta,0) = \delta(\theta)$, can be presented as a sum of angular harmonics:

$$n(\theta,t) = \frac{1}{2\pi} + \frac{1}{\pi}\sum_{k=1}^{\infty} \exp\left(-\frac{Dk^2 t}{a^2}\right)\cos(k\theta). \tag{43}$$

Assuming that the detector is located at $\theta = \pi$, we find the following expression for the spin density:

$$S_x(t) = \frac{1}{2\pi}\sum_{k=-\infty}^{\infty}(-1)^k \exp\left(-\frac{Dk^2 t}{a^2} - \frac{t}{\tau_s}\right)\cos\omega_L t. \tag{44}$$

Integration of $S_x(t)$ over time yields the nonlocal resistance in the form of the infinite sum

$$R(\omega_L) = R_0 \sum_{k=-\infty}^{\infty} \frac{1 + \frac{Dk^2\tau_s}{a^2}}{\left(1 + \frac{Dk^2\tau_s}{a^2}\right)^2 + \omega_L^2\tau_s^2}. \tag{45}$$

A closed expression for $R(\omega_L)$ can be obtained with the use of the identity

$$\sum_{k=-\infty}^{\infty}\frac{(-1)^k(1+k^2\lambda^2)}{(k^2\lambda^2+1)^2+z^2} = \frac{2}{(1+z^2)^{1/2}} \times\left[\frac{x\sinh(x)\cos(y) - y\sin(y)\cosh(x)}{\cosh 2x - \cos 2y}\right], \tag{46}$$

where

$$x = \frac{\pi}{\lambda}\sqrt{\frac{\sqrt{1+z^2}+1}{2}},\ y = \frac{\pi}{\lambda}\sqrt{\frac{\sqrt{1+z^2}-1}{2}}. \tag{47}$$

Expressing the nonlocal resistance with the help of Eq. (46) requires the following identifications:

$$z = \omega_L\tau_s,\quad \lambda = \frac{(D\tau_s)^{1/2}}{a}. \tag{48}$$

The prefactor π/λ in Eq. (47) is equal to $2\pi a/(4D\tau_s)^{1/2}$, which is the circumference of the loop in the units of spin-diffusion length. The identity Eq. (46) suggests that nonlocal resistance depends on parameter y in an oscillatory fashion. To clarify the physical meaning of these oscillations consider the limit of weak fields, $z \ll 1$, so that the precession angle of spin, $\delta\varphi$, during the time τ_s is small. In this limit, the parameter y can be cast in the form

$$y\big|_{z\ll 1} \approx \frac{2\pi a}{(D\tau_s)^{1/2}}\delta\varphi. \tag{49}$$

The first factor in Eq. (49) can be interpreted as a number of intervals, each having a length equal to the spin-diffusion length, covered by an electron before it makes a full loop. Since the spin is rotated by $\delta\varphi$ over each interval, the parameter y can be interpreted as a full rotation angle for the whole loop. Then the periodicity of nonlocal resistance corresponds to this full angle being π, 2π, and so on.

To interpret the oscillations in strong fields, $z \gg 1$, we rewrite the parameter y as

$$y\big|_{z\gg 1} \approx \frac{2\pi a}{(D/\omega_L)^{1/2}}. \tag{50}$$

The denominator in Eq. (50) has the meaning of the length traveled during one Larmour precession period. The fact that $\mathcal{R}$ is sensitive to whether the circumference contains integer or half-integer number of these lengths can be interpreted as an effect of finite step size in the random walk. Naturally, these

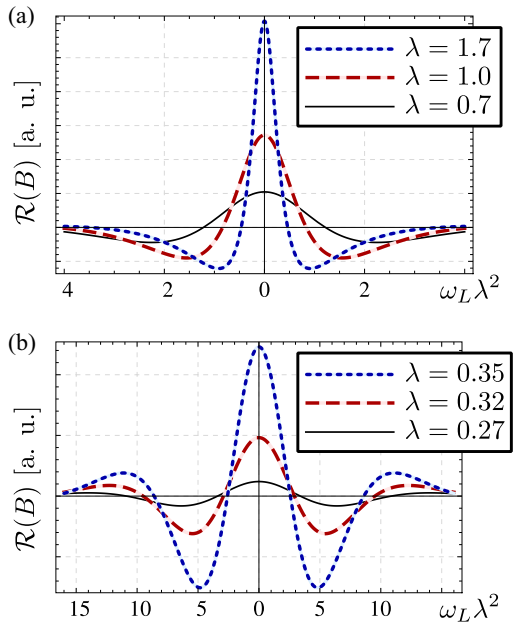

FIG. 5. (Color online) (a) Evolution of the Hanle curves $\mathcal{R}(\omega_L)$ with radius a. The curves are plotted from Eq. (46) for three values of the dimensionless loop radius $\lambda^{-1} = a/(D\tau_s)^{1/2}$. Dotted, dashed, and solid lines correspond to $\lambda = 1.7$, 1, and 0.7, respectively. (b) Same as (a) for the high-temperature domain $\lambda = 0.35$ (dotted), 0.32 (dashed), and 0.27 (solid).

oscillations are suppressed exponentially, since at strong fields we have $x \approx y$.

Suppose now that the temperature is low, so that τ_s is long. This means that, before the spin orientation is forgotten, the particle performs many loops, so that density $n(\theta)$ is nearly homogeneous. This, in turn, suggests that the Hanle profile is unaffected by the diffusion, and has a Lorentzian shape. Plotting $\mathcal{R}(\omega_L)$ from Eq. (46) indicates that a Lorentzian shape is achieved only for very small loops, such that $\lambda \gtrsim 40$. For moderate values of $\lambda \sim 1$, i.e., for higher temperatures, the Hanle profiles are non-Lorentzian, but rather resemble $\mathcal{R}(\omega_L)$ for a long wire, as illustrated in Fig. 5(a). Finally, for "high" temperatures corresponding to $\lambda \sim 0.3$, see Fig. 5(b), the Hanle curves develop oscillations discussed above, while the magnitude of $\mathcal{R}(\omega_L)$ drops rapidly with decreasing λ.

VI. DISCUSSION

(1) The fact that experimental Hanle curves are amazingly robust motivated us to investigate whether the charge-transport characteristics could be inferred from their shapes. Namely, in a system of two coupled wires, the tunneling time, τ_t, between the wires is a parameter that does not depend on spin. Still, as it is seen in Fig. 3, the Hanle curves calculated for a given wire, $\mathcal{R}_{11}$, and between the wires, $\mathcal{R}_{12}$, have visibly different widths. The difference in widths is governed by the ratio Δ_t/Δ_s of fundamental "band-structure" parameters. Thus this ratio can be inferred from the comparison of these widths. Also, Δ_s can, in principle, be inferred independently from the shape of $\mathcal{R}_{11}$. The possibility of such an extraction of tunnel splitting is facilitated by the fact that τ_s falls off with increasing temperature dramatically (as T^{-3} for the Dyakonov-Perel mechanism [1]), whereas τ_t varies slowly. This rapid change of τ_s with temperature allows for a "dimensional crossover" between 0D and 1D statistics of diffusion paths within the same ring-shaped sample, see Fig. 2(c). This crossover manifests itself not only in the width but also in the shape of Hanle curve, which becomes a Lorentzian at low temperatures.

Note that, in principle, there is an alternative way to infer the bare tunnel splitting Δ_t experimentally that does not involve spin, namely, the luminescence measurements. For the case of two tunnel-coupled quantum wells [23], one well is excited, while the luminescence is measured from both wells. Luminescence from the second well emerges after time τ_t, while the width of the luminescence spectrum yields τ^{-1}. In this way, $\Delta_t = (\tau\tau_t)^{-1/2}$ can be found.

(2) In a sense, our quest to reveal the statistics of diffusion paths through the Hanle curves is in line with attempts taken to unravel this statistics from the weak-localization correction to the conductivity, $\Delta\sigma$ of a 2D sample [24,25].

The Hanle profile comes from multiplying the diffusive propagator by $\cos\omega_L t$ and integrating over time. Similarly, the expression for $\Delta\sigma$ comes from multiplying the diffusive return probability by $\cos 2\pi\Phi(t)$ where $\Phi(t)$ is the flux (in the unit of the flux quantum) through the area covered by the diffusing particle after time t and integrating over t. Thus both $\mathcal{R}$ and $\Delta\sigma$ are essentially the Fourier transforms of the diffusion propagator. The role of the spin-flip time τ_s in spin transport is played by the phase-breaking time in magnetoresistance.

In fact, a rapid decay of the phase-breaking time with temperature was also exploited previously in the transport studies [26,27] to demonstrate the dimensional crossover from quasi-2D to purely 3D diffusion. It should be noted, however, that while weak-localization relying on the spatial coherence of electrons shows up only at low temperatures, the Larmour precession survives at high temperatures and gives rise to the Hanle curve.

(3) Throughout the paper we considered a two-wire geometry. Another class of structures to which our results might be applicable is tunnel-coupled graphene layers. It was previously demonstrated [11,15,16,28,29] that a single layer of graphene can be used as a channel for nonlocal spin-transport measurements. A possibility to fabricate two tunnel-coupled layers was also demonstrated very recently [30–33]. The structures [30–33] were fabricated in order to realize the vertical gate-controlled graphene heterostructures.

(4) We considered the spin-current distribution in a loop geometry. Very recently [34] a measurement of nonlocal spin transport in a loop geometry has been reported. The importance of findings of Ref. [34] is that the result of conversion of a spin current into a charge current was revealed not through the voltage buildup in an open-circuit geometry but rather by directly measuring the circulation of current in the loop.

(5) The bridge between two channels shown in Fig. 2(b) can be viewed as a boundary condition for the diffusion equation that changes the random-walk trajectories leading to a modified shape of the Hanle curves. The origin of such a boundary condition can be simply a finite length of the channel. This situation was recently considered theoretically [35]. In accord with our findings, the result of decreasing the channel length is the crossover of the Hanle shape to a Lorentzian.

ACKNOWLEDGMENTS

This work was supported by NSF through MRSEC DMR-1121252. E.M. acknowledges support from the Department of Energy, Office of Basic Energy Sciences, Grant No. DE-FG02-06ER46313.

APPENDIX

In order to substantiate the statement made in Sec. III that the concentration profile in the second wire,

$$n_2(L_2,t) \propto \int_0^t dt_1\ P_{L_2}(t-t_1)P_{L_1}(t_1), \tag{A1}$$

does not depend on the position L_1 of the bridge, it is convenient to use the Fourier representation of the diffusive propagators P_{L_1} and P_{L_2}. In this representation, Eq. (A1) acquires the form

$$n_2 \propto \int_0^t dt_1 \left[\int \frac{dq_2}{2\pi} \exp\left(-Dq_2^2(t-t_1)+iq_2L_2\right) \int \frac{dq_1}{2\pi} \exp\left(-Dq_1^2t_1+iq_1L_1\right)\right]. \tag{A2}$$

Performing the time integration, we get

$$n_2 \propto \int \frac{dq_1}{2\pi} \int \frac{dq_2}{2\pi} \exp\left(iq_1L_1+iq_2L_2\right) \left(\frac{\exp\left(-Dq_1^2t\right)-\exp\left(-Dq_2^2t\right)}{q_1^2-q_2^2}\right). \tag{A3}$$

The sum, $L = L_1 + L_2$, which is the total length, does not depend on the position of the bridge, while the difference $l = L_1 - L_2$ is fully determined by the position of the bridge. In order to decouple L and l, we introduce the new variables

$$u = q_1 + q_2, \quad v = q_1 - q_2, \tag{A4}$$

so that the integral (A3) assumes the form

$$n_2 \propto \int \frac{du}{u} \exp\left(-\frac{Dtu^2}{4}+i\frac{L}{2}u\right) \int \frac{dv}{v} \exp\left(-\frac{Dtv^2}{4}+i\frac{l}{2}v\right) \sinh\left(\frac{Dtuv}{2}\right). \tag{A5}$$

Independence of n_2 on the position of the bridge implies that $\partial n_2/\partial l = 0$. Differentiating Eq. (A5) with respect to l, we get

$$\frac{\partial n_2}{\partial l} \propto \int \frac{du}{u} \exp\left(-\frac{Dtu^2}{4}+i\frac{L}{2}u\right) \int dv\ \exp\left(-\frac{Dtv^2}{4}+i\frac{l}{2}v\right) \sinh\left(\frac{Dtuv}{2}\right). \tag{A6}$$

Note that the internal integral in Eq. (A6) can be readily evaluated

$$\int dv\ \exp\left(-\frac{Dtv^2}{4}+i\frac{l}{2}v\right) \sinh\left(\frac{Dtuv}{2}\right) \propto \exp\left(\frac{Dtu^2}{4}\right) \sin\frac{lu}{2}. \tag{A7}$$

This allows us to express $\partial n_2/\partial l$ as a single integral:

$$\frac{\partial n_2}{\partial l} \propto \int \frac{du}{u} \exp\left(\frac{iLu}{2}\right) \sin\frac{lu}{2} = \frac{1}{2}\int du \frac{\sin\frac{(L+l)u}{2} - \sin\frac{(L-l)u}{2}}{u}. \tag{A8}$$

From the identity

$$\int_{-\infty}^{\infty} \frac{ds}{s} \sin\alpha s = \pi\ \mathrm{sign}(\alpha), \tag{A9}$$

we conclude that indeed $\partial n_2/\partial l$ is zero *as long as* $l < L$. Thus the concentration, $n_2(L_2,t)$, does not depend on the position of the bridge only when the bridge is located between the injector and the detector.

[1] M. I. Dyakonov and V. I. Perel, Sov. Phys. Solid State **13**, 3023 (1971).
[2] R. R. Parsons, Phys. Rev. Lett. **23**, 1152 (1969).
[3] A. I. Ekimov and V. I. Safarov, Pis'ma Zh. Eksp. Teor. Fiz. **12**, 293 (1970) [JETP Lett. **12**, 198 (1970)].
[4] A. I. Ekimov, D. Z. Garbuzov, and V. I. Safarov, Pis'ma Zh. Eksp. Teor. Fiz. **13**, 36 (1971) [JETP Lett. **13**, 24 (1971)].
[5] R. I. Dzhioev, V. L. Korenev, B. P. Zakharchenya, D. Gammon, A. S. Bracker, J. G. Tischler, and D. S. Katzer, Phys. Rev. B **66**, 153409 (2002).
[6] M. Johnson and R. H. Silsbee, Phys. Rev. Lett. **55**, 1790 (1985).
[7] M. Johnson and R. H. Silsbee, Phys. Rev. B **37**, 5312 (1988).
[8] F. J. Jedema, A. T. Filip, and B. J. van Wees, Nature (London) **410**, 345 (2001).
[9] I. Appelbaum, B. Huang, and D. Monsma, Nature (London) **447**, 295 (2007).
[10] X. Lou, C. Adelmann, S. A. Crooker, E. S. Garlid, J. Zhang, S. M. Reddy, S. D. Flexner, C. J. Palmstrøm, and P. A. Crowell, Nat. Phys. **3**, 197 (2007).

[11] N. Tombros, C. Jozsa, M. Popinciuc, H. T. Jonkman, and B. J. van Wees, Nature (London) **448**, 571 (2007).
[12] S. Watanabe, K. Ando, K. Kang, S. Mooser, Y. Vaynzof, H. Kurebayashi, E. Saitoh, and H. Sirringhaus, Nat. Phys. **10**, 308 (2014).
[13] K. Kasahara, Y. Fujita, S. Yamada, K. Sawano, M. Miyao, and K. Hamaya, Appl. Phys. Express **7**, 033002 (2014).
[14] K. Olejník, J. Wunderlich, A. C. Irvine, R. P. Campion, V. P. Amin, J. Sinova, and T. Jungwirth, Phys. Rev. Lett. **109**, 076601 (2012).
[15] T. Yamaguchi, Y. Inoue, S. Masubuchi, S. Morikawa, M. Onuki, K. Watanabe, T. Taniguchi, R. Moriya, and T. Machida, Appl. Phys. Express **6**, 073001 (2013).
[16] A. Dankert, M. V. Kamalakar, J. Bergsten, and S. P. Dash, Appl. Phys. Lett. **104**, 192403 (2014).
[17] For details of the fabrication, see M. C. Prestgard and A. Tiwari, Appl. Phys. Lett. **104**, 122402 (2014).
[18] We adopt the simplest diffusion description of transport and neglect the complications arising from localized states in the channel, Y. Song and H. Dery, Phys. Rev. B **81**, 045321 (2010), and from resonant-tunneling injection from a ferromagnet, Y. Song and H. Dery, Phys. Rev. Lett. **113**, 047205 (2014).
[19] In a superlattice with a period a and miniband width Δ, the diffusion coefficient is equal to $\frac{a^2}{\tau_t} = a^2\Delta^2\tau$, see C. Mauz, A. Rosch, and P. Wölfle, Phys. Rev. B **56**, 10953 (1997), the diffusion coefficient in a multilayer system.
[20] O. E. Raichev and P. Vasilopoulos, J. Phys. Condens. Matter **12**, 6859 (2000).
[21] S. A. Crooker, M. Furis, X. Lou, C. Adelmann, D. L. Smith, C. J. Palmstrøm, and P. A. Crowell, Science **309**, 2191 (2005).
[22] T. Sasaki, T. Oikawa, T. Suzuki, M. Shiraishi, Y. Suzuki, and K. Noguchi, IEEE Trans. Magn. **46**, 1436 (2010).
[23] D. Y. Oberli, J. Shah, T. C. Damen, C. W. Tu, T. Y. Chang, D. A. B. Miller, J. E. Henry, R. F. Kopf, N. Sauer, and A. E. Di Giovanni, Phys. Rev. B **40**, 3028 (1989).
[24] G. M. Minkov, A. V. Germanenko, V. A. Larionova, S. A. Negashev, and I. V. Gornyi, Phys. Rev. B **61**, 13164 (2000).
[25] G. M. Minkov, S. A. Negashev, O. E. Rut, A. V. Germanenko, O. I. Khrykin, V. I. Shashkin, and V. M. Daniltsev, Phys. Rev. B **61**, 13172 (2000).
[26] A. K. Savchenko, A. S. Rylik, and V. N. Lutskii, Zh. Eksp. Teor. Fiz. **85**, 2210 (1983).
[27] A. M. Gilbertson, A. K. M. Newaz, W.-J. Chang, R. Bashir, S. A. Solin1, and L. F. Cohen, Appl. Phys. Lett. **95**, 012113 (2009).
[28] C. Józsa, M. Popinciuc, N. Tombros, H. T. Jonkman, and B. J. van Wees, Phys. Rev. Lett. **100**, 236603 (2008); Phys. Rev. B **79**, 081402 (2009).
[29] M. H. D. Guimarães, A. Veligura, P. J. Zomer, T. Maassen, I. J. Vera-Marun, N. Tombros, and B. J. van Wees, Nano Lett. **12**, 3512 (2012).
[30] L. Britnell, R. V. Gorbachev, R. Jalil, B. D. Belle, F. Schedin, A. Mishchenko, T. Georgiou, M. I. Katsnelson, L. Eaves, S. V. Morozov, N. M. R. Peres, J. Leist, A. K. Geim, K. S. Novoselov, and L. A. Ponomarenko, Science **335**, 947 (2012).
[31] T. Georgiou, R. Jalil, B. D. Belle, L. Britnell, R. V. Gorbachev, S. V. Morozov, Y.-J. Kim, A. Gholinia, S. J. Haigh, O. Makarovsky, L. Eaves, L. A. Ponomarenko, A. K. Geim, K. S. Novoselov, and A. Mishchenko, Nat. Nanotechnol. **8**, 100 (2013).
[32] S. Bertolazzi, D. Krasnozhon, and A. Kis, ACS Nano **7**, 3246 (2012).
[33] S. Kim, D. H. Shin, C. O. Kim, S. S. Kang, J. M. Kim, C. W. Jang, S. S. Joo, J. S. Lee, J. H. Kim, S.-H. Choi, and E. Hwang, ACS Nano **7**, 5168 (2013).
[34] Y. Omori, F. Auvray, T. Wakamura, Y. Niimi, A. Fert, and Y. Otani, Appl. Phys. Lett. **104**, 242415 (2014).
[35] M. Wojtaszek, I. J. Vera-Marun, and B. J. van Wees, Phys. Rev. B **89**, 245427 (2014).